Structure and Properties of Albite Melt at High Pressures

Suraj K. Bajgain* and Mainak Mookherjee

Department of Earth, Ocean and Atmospheric Sciences, Florida State University, Tallahassee, Florida 32306, United States

Ⓢ *Supporting Information*

ABSTRACT: We have used first-principles molecular dynamics simulation to examine the high-pressure behavior of an aluminosilicate melt with albite stoichiometry ($NaAlSi_3O_8$). We have explored the equation of state and transport properties up to a pressure of 25 GPa and over a range of temperatures (2500−4000 K). Our results show that upon compression of up to 5 GPa, the initial densification in an albite melt occurs by the reduction of the T−O−T bond angle; however, the Si−O coordination remains virtually unchanged. Upon compression beyond 5 GPa, the densification occurs via changes in the T−O coordination. We also find that at lower isotherms, i.e., 2500−3000 K, the viscosity decreases upon compression and there is a concomitant enhancement of the diffusivity of the network-forming tetrahedral cations (silicon/aluminum) and oxygen anions. However, there is a reversal in the trend of viscosity and diffusivity upon further compression. For all of the temperatures explored in this study, at higher pressures, i.e., >10 GPa, the viscosity increases with increasing pressure, whereas the diffusivity decreases with increasing pressures. This behavior of the melt transport property at high pressures is expected, contrary to the observed behavior of melt transport at low pressures and low temperatures. The pressure-dependent anomalous transport properties are very likely related to the formation of the 5-fold coordinated aluminum ions that have a shorter lifetime compared to those of the more stable 4-fold and 6-fold coordinated units.

KEYWORDS: *albite melt, high pressures, first-principles molecular dynamics, diffusion, viscosity, melt mobility*
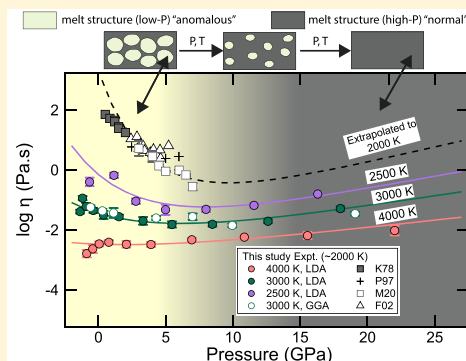
■ INTRODUCTION

Albite ($NaAlSi_3O_8$) is the sodium end member composition for both plagioclase feldspar ($Ca_xNa_{1−x}Al_{1+x}Si_{3−x}O_8$) and alkali feldspar ($K_xNa_{1−x}AlSi_3O_8$) (where $0 < x < 1$), which are important constituents in igneous rocks/silicate melts with silicic, intermediate, and mafic compositions. Albite-rich compositions may also have been an important constituent in tonalite−trondhjemite−granodiorite (TTG) magmas in the early history of the Earth, i.e., Archean, since TTG complexes often contain 30−40% albite.[1,2] Owing to its ubiquitous presence in igneous rocks, and fundamental importance in silica-rich and intermediate magma genesis, the melting of albite has received considerable attention.[3−6] It is clear that better constraints on the structure and property of albitic melt at ambient conditions as well at high pressures would improve our understanding of the properties and behavior of silicate melts such as granodiorites and andesites, which are often associated with present-day subduction settings. The ability of silicate melts to segregate from its source depends strongly on the melt properties, of which viscosity and density are the most important.[7,8] There exists significant literature on albite melts and glasses; however, the experimental data on the density of albite melts at relevant high pressures and temperatures are often derived by summing the partial molar volumes from experiments conducted at ambient pressures.[9−11] The pressure derivative of the bulk modulus and the heat capacity have been estimated using the fusion curve and calorimetric data.[12] The structure of quenched albite glasses has been explored using spectrosco-

py.[13−16] These structural investigations have documented the changes in the coordination environment of network-forming cations at high pressures. However, these are often not in situ measurements, and the speciation information is often affected by the thermal and quench history of the annealed glass sample.

Similar to fundamental properties such as density, the pressure dependence of the viscosity of albite melts has also been explored but is limited to low-pressure regime.[17−20] Owing to the limited range of pressures explored, these earlier experiments differ in the observed trend of viscosity with pressure. Few experiments report an anomalous behavior, i.e., viscosity decreases with pressure and reaches a minimum before increasing upon further compression,[19,20] while other experiments show a decrease of viscosity upon compression up to 7 GPa.[17] The explored range of pressure limits our ability to understand how viscosity evolves with increasing pressure. So far, the existing molecular dynamics simulation results on albite melt are based on classical semiempirical potentials, and the molecular dynamics (MD) simulations explored the thermodynamics and self-diffusion coefficients of albite melt at temperatures >3000 K.[21,22]

Thus, to better understand the high-pressure properties of silicate melts where albite end member compositions might play

an important role, we explore the equation of state and transport properties of albite melt at high pressures. We relate the observed change in bulk thermodynamic and transport properties of the melt with the atomistic scale changes in the melt structures using first-principles molecular dynamics (FPMD) simulations.

■ METHOD

We examine the structure and properties of $NaAlSi_3O_8$ melt using first-principles molecular dynamics (FPMD) simulation with local density approximation (LDA).[23] FPMD has been extensively used to examine the properties of geophysically relevant liquids and melts.[24−27] In FPMD simulations, the interatomic forces at each time step are computed using density functional theory (DFT) as implemented in the Vienna ab initio simulation package (VASP).[28−30] In all our simulations, we used a time step of 0.5 fs (1 fs = 10^{-15} s). We performed the simulations at a constant temperature using Nosé thermostat.[31] We used the projector-augmented wave (PAW) method with a plane wave energy cutoff (E_{cut}) of 450 eV in the canonical NVT ensemble.[32,33] In our simulations, we sampled the Brillouin zone at the $\Gamma = 0$.

In our simulations, we have used an albite crystal structure with a triclinic unit cell as an initial guess and strained the triclinic unit cell homogeneously to a cubic cell and melted the crystal at high temperatures of ∼6000 K. After this, it was cooled along an isochore to lower temperatures of 4000, 3000, and 2500 K. Homogeneous straining of the lower symmetry unit cells of crystalline matter to a cubic unit cell has been adopted in previous studies.[24,34] We explored albite melt with eight formula units of $NaAlSi_3O_8$ (104 atoms). For each isotherm, we explored pressures of up to 25 GPa, and melts were simulated at a constant volume (density). Our initial simulation cell size of ∼1393.61 $Å^3$ (104.91 cm^3/mol) was used as a reference volume (V_{ref}), and the corresponding reference density, $\rho_{ref} = 2.50$ g cm^{-3}. At a constant density of 2.19 g cm^{-3} and 4000 K, we also explored four different system sizes with 52 atoms, 104 atoms, 156 atoms, and 208 atoms, respectively. The calculated energy, pressure, structure, and transport properties remain largely unaffected by the system size (Supporting Figures S1−S3). We do note that the time required for the convergence of energy and pressure for larger system size is faster. However, the total simulation time increases nonlinearly with the size of the system (Supporting Figure S1). We also examine the role of exchange−correlation by exploring generalized gradient approximation (GGA) pseudopotential for the 3000 K isotherm[35] (Supporting Figure S4, Table S1, and Datasheet).

We examined the radial distribution function (RDF) and mean square displacement to ascertain whether the system attained a liquid state (Supporting Figures S2, S3, and S5−S7). Upon attaining the liquid state, the RDF exhibits a short- to mid-range order and long-range disorder (Supporting Figures S2 and S5). The coordination number for a pair of atoms is determined by integrating the first peak of the RDF up to the first minima, i.e., r_{min} (Supporting Figure S2). Similarly, upon attaining a liquid state, the mean square displacement (MSD) shows a linear increase with time, in contrast with the solid condensed matter where MSD remains rather insensitive with the elapsed simulation time (Supporting Figure S6). We evaluated the log−log plot of MSD vs time at 2500 K to ascertain a slope of unity, and we also note that the MSD exceeded 10 $Å^2$ within our simulation time, indicating that the melt exhibits an ergodic behavior (Supporting Figure S7).

We use the blocking method to determine the average energy and pressures for each simulation volume[36] (Supporting Figures S1, S5 and Datasheet). We use a finite cutoff energy (E_{cut} = 450 eV) for our simulation and thus we have made corrections in pressure (P_{Pulay}), as in (eq 1)

$$P(V) = P_{VASP}(V) + P_{Pulay}(V) \tag{1}$$

We choose the finite energy cutoff for longer simulation time scales for a better constraint on the transport properties. The $P_{Pulay}(V)$ is the pressure difference between the higher energy cutoff and the finite energy cutoff used in this study and is expressed as (eq 2)

$$P_{Pulay}(V) = P_{750\ eV} - P_{450\ eV} \tag{2}$$

where P_{750} and P_{450} eV are the pressures from simulations using the energy cutoffs of 750 and 450 eV, respectively. We estimate the self-diffusion coefficient of the corresponding ions from the motion of individual ions at each simulation step using the Einstein formulation (eq 3)

$$D = \lim_{n \to \infty} \frac{1}{6t}\left(\frac{1}{N} \sum_{i=1}^{N} \{r_i[t + t_0] - r_i[t_0]\}^2 \right) \tag{3}$$

The terms inside the parentheses refer to the mean square displacement, where r_i and $r_i[t + t_0]$ refer to the position of the ith atom at time t_0 and its position after an additional time t, respectively.

We estimate the viscosity (η) of albite melt using the Green−Kubo relation[33,37]

$$\eta = \frac{V}{10k_B} \int_{\infty}^{0} \left\langle \left(\sum_{\alpha\beta} P_{\alpha\beta}(t + t_0) \times P_{\alpha\beta}(t_0) \right) \right\rangle dt \tag{4}$$

where $P_{\alpha\beta}$ is the symmetrized and traceless portion of the stress tensor $\sigma_{\alpha\beta}$ from each simulation step

$$P_{\alpha\beta} = \frac{1}{2}(\sigma_{\alpha\beta} + \sigma_{\beta\alpha}) - \frac{1}{3}\delta_{\alpha\beta}\left(\sum_{\lambda} \sigma_{\lambda\lambda} \right) \tag{5}$$

In eq 5, $\delta_{\alpha\beta}$ is the Kronecker delta. For estimating the η, we use the off-diagonal and diagonal components of stress tensor with different weighting factors of 1 and 4/3, respectively.[38,39] The integrand is the stress autocorrelation function (ACF). Normalized stress ACF decreases with time, and viscosity is calculated after the ACF reaches a steady state and viscosity remains relatively constant with time (Supporting Figure S6).

■ RESULTS

Equation of State. We find that the pressure and volume data across all of the isotherms for albite can be described with a Mie−Grüneisen thermal equation of state formalism

$$P(V, T) = P(V, T_{ref}) + \left(\frac{dP}{dT} \right)_V (T - T_{ref}) \tag{6}$$

where $\left(\frac{dP}{dT} \right)_V = \alpha K_T$, α refers to the coefficient of thermal expansivity, and K_T refers to the isothermal bulk modulus. We have used the pressure at 2500 K isotherm as the reference pressure $P(V, T_{ref})$. The pressure−volume results of the reference isotherm $(T_{ref} = 2500$ K) can be described by the third-order Birch−Murnaghan (BM3) equation of state formalism (Figure 1 and Table 1)
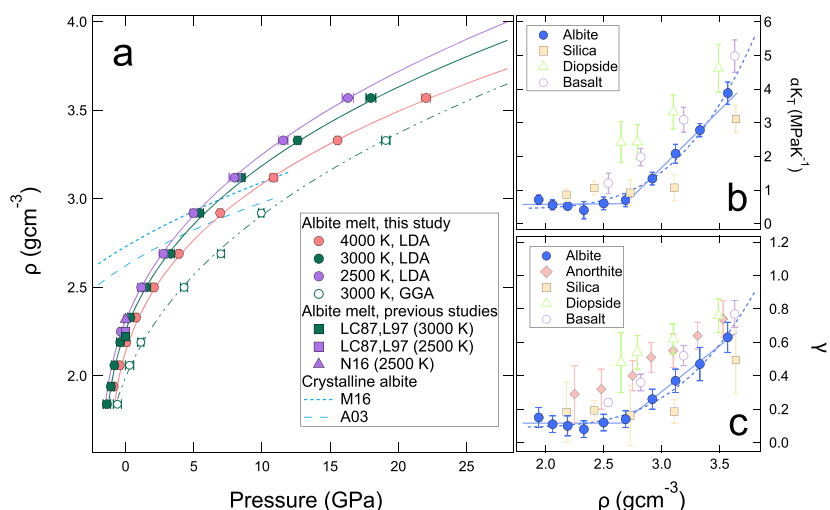
Figure 1. (a) Pressure–density relation for albite melts along 4000 K (red-filled symbols), 3000 K (green-filled symbols), and 2500 K (purple-filled symbols). Lines represent the third-order BM equation of state (eq 7) at reference isotherm (T_{ref} = 2500 K) and Mie–Grüneisen thermal equation of state (eq 6) fit for other isotherms. Filled purple and green squares represent the density of albite melt at 2500 and 3000 K determined using a partial molar volume of oxides (L87 and L97).[9,10] Filled purple triangle shows the density of albite melt at 2500 K from the previous classical MD simulation (N16).[22] Green open symbols are GGA results at 3000 K. Green dashed line represents the third-order BM equation of state (Supporting Table S1). Dashed cyan lines represent the densities for crystalline albite from a static calculation using LDA (M16) and from single crystal X-ray diffraction studies at room temperature (A03).[60,73] (b) Plot of the thermal pressure coefficient $\left(\frac{dP}{dT}\right)_V = \alpha K_T$ as a function of density (blue solid symbols) fitted with the relation $\left(\frac{dP}{dT}\right)_V = a + b\,e^{c \times u}$, where $u = \frac{V}{V_{ref}} = \frac{\rho_{ref}}{\rho}$, and a = 0.45 MPa/K; b and c are 1668.50 MPa/K and −8.80, respectively. (c) Grüneisen parameter calculated at each density (volume) for albite melt compared with that for other silicate melts.[45,58,66,67] Symbols are the same as panel (b). In panels (b) and (c), symbols indicate the mean values at each density over the temperature range of 2500−6000 K and dashed lines represent the fitted values (eq 10 for Grüneisen parameter fit). Lines in panels (b) and (c) indicate the low-pressure and high-pressure trends in $\left(\frac{dP}{dT}\right)_V$ and γ.

Table 1. Third-Order Birch–Murnaghan (BM3) Equation of State Fit Parameters for Albite (NaAlSi$_3$O$_8$) Melt at 2500 K[a]

	albite melt		anorthite melt	crystalline albite
	this study	previous studies		
ρ_0 (g cm^{-3})	2.31 ± 0.04	2.32^c, 2.25 ± 0.02^{d,e}	2.39 ± 0.01^h	2.62 ± 0.04^j, 2.62 ± 0.05^l
K_0 (GPa)	11.83 ± 2.25	16.75 ± 0.89^f	11.5 ± 0.3^h	53.8±0.9^j, 52.3±0.9^l
K_0'	5.31 ± 0.70	10.8 ± 1.5^g	6.8 ± 0.6^h	6 ± 0.6^j, 8.8 ± 0.6^l
γ at 0 GPa	0.11	0.21^c	0.33 ± 0.2^i	
α at 0 GPa (×10^{-5} K^{-1})	4.84	7.98^c, 3.64^e	9.2 ± 0.8^i	2.68^k
β_T at 0 GPa (GPa^{-1})	0.085, 0.077^b	0.088^c, 0.060^f		0.017^g

^{a}We have compared our results with the previous study on albite and anorthite melts. In addition, we have also compared the equation of state parameter for crystalline albite. Note: italicized numbers refer to the results at temperatures other than 2500 K. ^{b}FPMD result for albite melt extrapolated to 1773 K. ^{c}Neilson et al. (2016).[22] Pair potential MD simulation results at 2500 K. ^{d}Lange (1997),[10] and Lange and Carmichael (1997). Experimental data extrapolated to 2500. ^{e}Lange (1996).[72] Experimental data extrapolated to 2500 K. ^{f}Kress et al. (1988).[11] Experimental data extrapolated to 2500 K. ^{g}Tenner et al. (2007).[12] Fusion curve analysis results at 1773 K. ^{h}Karki et al. (2011).[47] FPMD with LDA for anorthite melt at 3000 K. ^{i}de Koker (2010).[58] FPMD with LDA for anorthite melt at 3000 K. α values are at 1830 K. ^{j}Angel (2003).[73] Single crystal X-ray diffraction study of crystalline albite. ^{k}Fei (1995).[74] Experimental data for high albite at 298 K. ^{l}Benusa et al. (2005).[75] Single crystal X-ray diffraction study of low albite.

$$P = \frac{3}{2} K_0 \left[\left(\frac{\rho}{\rho_0}\right)^{7/3} - \left(\frac{\rho}{\rho_0}\right)^{5/3} \right]$$
$$\times \left\{ 1 + \frac{3}{4}(K_0' - 4)\left[\left(\frac{\rho}{\rho_0}\right)^{2/3} - 1 \right] \right\} \quad (7)$$

We find that the density of NaAlSi$_3$O$_8$ melt at 2500 K and ambient pressure is 2.31 ± 0.04 g cm^{-3}. Our calculated density at ambient pressure is also comparable with the density from the previous classical MD simulation of albite melt.[22] The ρ_0 results based on LDA are slightly higher than the zero pressure–density (2.25 ± 0.02 g cm^{-3}) predicted from the summation of the

experimentally determined partial molar volumes of oxides at similar conditions.[9,10] The slight discrepancy is likely due to the LDA pseudopotential, which tends to overbind, i.e., LDA volumes (densities) tend to be lower (higher) than experimental results.[40] For the 3000 K isotherm, the zero pressure–density predicted from LDA (ρ_0^{LDA}) is greater than the experimental density (ρ_0^{exp}) results by 2%, whereas the density predicted from GGA (ρ_0^{GGA}) is smaller than the experimental (ρ_0^{exp}) results by 10%. The experimental density (ρ_0^{exp}) is estimated by summing the molar volume of oxides extrapolated to 3000 K (Supporting Figure S4 and Table S1).[9,10] We note that the choice of exchange–correlation, i.e., GGA vs. LDA pseudopotential, on the structure and transport properties of the melt is within the

uncertainties of the study. Since zero pressure–density predicted from LDA (ρ_0^{LDA}) is in better agreement with experiments, we chose the LDA method to explore all of the isotherms between 2500 and 4000 K.

We find that both pressure and energies increase linearly with increasing temperature. Thus, at a constant volume (density), we can determine isochoric heat capacity (C_V) and Grüneisen parameter (γ) using the following relationship

$$C_V = \left(\frac{dE}{dT}\right)_V \tag{8}$$

$$\gamma = \frac{V}{C_V}\left(\frac{dP}{dT}\right)_V \tag{9}$$

The Grüneisen parameter (γ) varies as a function of density, with γ being 0.15 at $\rho = 1.94$ g cm^{-3} and slightly reduces to 0.08 at $\rho = 2.33$ g cm^{-3}. Upon further compression, γ increases with increasing density (Figure 1). For the entire range of density explored in this study, γ varies nonlinearly with density (volume) and can be described using the following relations

$$\gamma = \gamma_{ref} + \gamma' \, e^{-\gamma'' \times u} \tag{10}$$

where $u = \frac{\rho_{ref}}{\rho}$ or $\frac{V}{V_{ref}}$, $\rho_{ref} = 2.50$ g cm^{-3} ($V_{ref} = 104.91$ cm^3 mol^{-1}), $\gamma_{ref} = 0.09 \pm 0.03$, $\gamma' = 240.4$, and $\gamma'' = 8.66 \pm 2.54$. We also find that the coefficient of thermal expansivity (α) decreases rapidly with increasing pressure up to ~5 GPa. Upon further compression, beyond 5 GPa, α is rather insensitive to pressure (Supporting Figure S8). The isothermal compressibility, $\beta_T \left(= -\frac{1}{V}\left(\frac{dV}{dP}\right)_T \right)$, also exhibits pressure dependence similar to α, i.e., β_T is 0.085 GPa^{-1} at 0 GPa and 2500 K and decreases rapidly with increasing pressure up to ~5 GPa (Supporting Figure S8 and Table 1). Comparing β_T of albite melt with crystalline albite clearly shows that the melt has a lower density at lower pressures, but the melt is also more compressible than its crystalline counterpart, which is likely to manifest into a density crossover at high pressure. For example, β_T for the melt at 1773 K (extrapolated) and 0 GPa is ~4–5 times larger than crystalline albite at similar conditions[12] (Table 1). Calculated thermodynamic properties at ambient pressure and 2500 K isotherm are in good agreement with the previous experimental results (Table 1).

We also determine the internal pressure (P_{int}) of liquid albite, which provides insights into the interatomic forces. Internal pressure is often expressed in terms of interatomic forces, $P_{int}^F = -\left(\frac{\partial E}{\partial V}\right)_T = P - T\left(\frac{\partial P}{\partial T}\right)_V$. It is very likely that P_{int}^F is related to the pressure-induced structural changes in the melt.[22] Our results show that upon compression, P_{int}^F increases along all isotherms (Figure 2). At low-pressure regime, $P_{int}^F < 0$. This is indicative of the attractive nature of the interatomic forces. Upon compression, $P_{int}^F > 0$, which indicates the repulsive nature of the interatomic forces.[22,41]

The potential energy of dense fluids can often be described by the Rosenfeld and Tarazona (RT) scaling,[42] where $E_{Potential} = a(V) + b(V)T^{3/5}$. The parameters, $a(V)$ and $b(V)$, can be expressed as a function of volume. The RT scaling has been successfully applied for the classical molecular dynamics simulation result on anorthite and albite melts.[22,43] We have also explored the RT scaling for our FPMD results on albite melt and find that at pressures greater than 2 GPa, the temperature
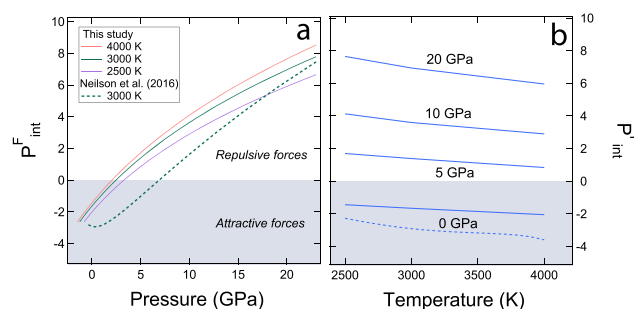
Figure 2. (a) Plot of internal pressure expressed as interatomic forces (P_{int}^F) with respect to pressure for 2500 K (purple lines), 3000 K (green lines), and 4000 K (red lines) isotherms. Green dashed line shows the P_{int}^F from the classical MD simulation at 3000 K.[22] (b) Temperature variation of P_{int}^F at a constant pressure of 0, 5, 10, and 20 GPa. Blue dashed line is the P_{int}^F at 1 bar from the classical MD simulation.[22]

dependence of the potential energy of albite melt can be well described by the RT scaling. For low-pressure data, i.e., pressures lower than 2 GPa, the applicability of the RT scaling is limited owing to the lack of data for lower-temperature isotherm (Supporting Table S2 and Figure S9).

Transport Properties. *Self-Diffusion.* The pressure dependence of self-diffusion coefficient is quite distinct at low-temperature isotherms, i.e., 2500 and 3000 K, compared to that of the higher-temperature isotherm at 4000 K. At 4000 K, the self-diffusivity of all ionic species decreases with increasing pressure (Figure 3). However, at lower temperatures, albite melt exhibits an anomalous behavior in the self-diffusivity of all ionic species except Na. For instance, at lower temperatures, the diffusivity of Al, Si, and O increases upon compression up to 6−8
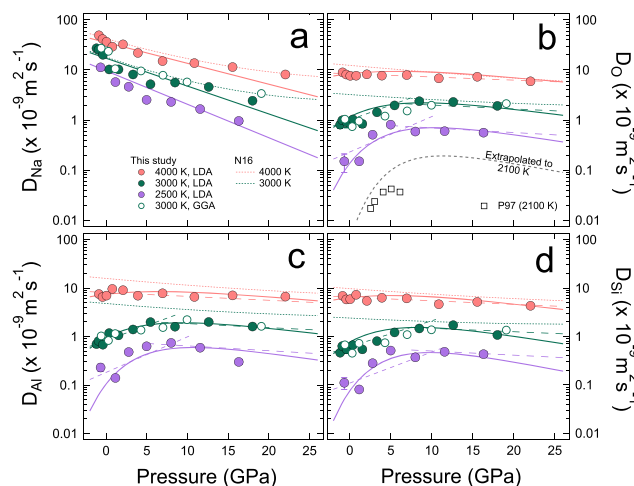
Figure 3. Pressure and temperature dependences of the self-diffusion of (a) Na, (b) O, (c) Al, and (d) Si ions for albite melts at 4000 K (red symbols), 3000 K (green symbols), and 2500 K (purple symbols) isotherms. Solid lines in panel (a) represent the Arrhenius model for Na diffusion (Table 2). Solid lines in panels (b−d) are the description of Al, Si, and O diffusions based on the model described in Tanaka (2003)[46] (eqs 11−14) to capture the anomalous pressure dependence of self-diffusion (Table 3, Supporting Text T1, and Figure S10). In panels (b−d), the dashed lines show two distinct Arrhenius fits to FPMD data at the low-pressure and high-pressure regimes (Table 2). Dotted lines represent the classical MD simulation results for albite melt along 4000 and 3000 K.[22] In panel (b), gray circles with line (P97) represent the experimental data for oxygen diffusivity at 2100 K.[20] Green open symbols in all panels represent GGA at 3000 K.

Table 2. Pre-Exponential Self-Diffusion Coefficient (D_{x0}), Activation Energies (E^*), and Activation Volumes (V^*) from the Arrhenius Relation for Albite (NaAlSi$_3$O$_8$) Melt

species (X)	composition	D_{x0} ($\times 10^{-9}$ m^2 s^{-1})	E^* (kJ mol^{-1})	V^* (cm^3 mol^{-1})	ref
Na	albite	314 ± 10	72 ± 1	3.2 ± 0.03	this study
			85		22
	jadeite	309 ± 32	77 ± 3	1.98±0.07	24
Al	albite	371 ± 32	127 ± 3	0.48 ± 0.05	this study[a]
		1686 ± 190	190 ± 4	−3.52 ± 0.14	this study[b]
			119		22
	jadeite	406 ± 89	125 ± 6	0.86±0.13	24[a]
		245 ± 128	136 ± 12	−2.3 ± 0.44	24[b]
Si	albite	328 ± 19	131 ± 2	0.41 ± 0.03	this study[a]
		1814 ± 574	199 ± 8	−3.06 ± 0.16	this study[b]
			140		22
	jadeite	251 ± 32	119 ± 3	0.97 ± 0.09	24[a]
		221 ± 125	143 ± 13	−2.49±0.43	24[b]
	dacite	40 ± 7	341 ± 19	−12.00 ± 1.00	44
O	albite	382 ± 18	127 ± 2	0.44 ± 0.02	this study[a]
		1535 ± 154	187 ± 2	−4.08 ± 0.08	this study[b]
			134		22
				−7.10 ± 1.00	21
	jadeite	328 ± 41	118 ± 3	0.62 ± 0.08	24[a]
		370 ± 179	144 ± 11	−2.69 ± 0.42	24[b]
	dacite	0.025 ± 0.0019	280 ± 12	−11.10 ± 0.70	44

[a]Fit parameters are obtained using all results from the 4000 K isotherm and the results from the high-pressure regime, where diffusivity decreases with increasing pressure, along 2500 and 3000 K isotherms. [b]Fit parameters are obtained using the results from the low-pressure regime, where diffusivity increases with increasing pressure, along 2500 and 3000 K isotherms.

GPa (Figure 3). However, upon further compression beyond 8 GPa, the diffusivity decreases. At lower isotherms, the self-diffusivity results could be described by two distinct pressure regimes: $P < 6-8$ GPa and $P > 8$ GPa. And both these pressure regimes follow the Arrhenius behavior. While at high pressures, we note a normal behavior of the pressure dependence of melt transport property, the lower-pressure region exhibits an anomalous behavior with the enhancement of diffusivity upon compression, i.e., a negative activation volume. Based on the LDA result on albite melt at pressures <6−8 GPa and low-temperature isotherms, i.e., 2500−3000 K, the activation volume for oxygen diffusion $V_O^* \sim -4.08$ cm^3 mol^{-1}. The previously reported experimental activation volume at slightly lower temperatures of 2100 K is ~ -8.30 cm^3 mol^{-1}.[20] Similar to the V_O^*, the activation volume for silicon diffusion $V_{Si}^* \sim -3.06$ cm^3 mol^{-1} is also greater than the experimental estimates at ~ 2100 K.[20,44] This discrepancy in the magnitude of the activation volume is consistent with the fact that at low pressures, the activation volume for the self-diffusivity of the oxygen ions is dependent on temperature[20,44] (Table 2). The activation volume gradually increases with an increasing temperature and changes sign at higher temperatures, i.e., $V^* < 0$ at low temperatures (2500−3000 K) and $V^* > 0$ at high temperature (4000 K). At high pressures, the diffusivity exhibits a normal trend across all temperatures, i.e., with a positive activation volume, $V^* > 0$ (Table 2 and Figure 3). A similar anomalous behavior of the P−T dependence of diffusivity has been observed in polymerized silicate melts across a diverse composition that includes albite, silica, jadeite, dacite, and basalt.[20,21,44,45] We note that the activation energies (E^*) for the diffusivity of Si, Al, and O atoms at low pressures are greater than those of high pressures (Table 2). For instance, the activation energy for oxygen diffusion at low pressures, E_O^*(loP), is 187 kJ

mol^{-1} and is greater than the activation energy for oxygen diffusion at high pressures, E_O^*(hiP) ~ 127 kJ mol^{-1}. Our results on E^* at high pressure and 2500−4000 K are comparable to the previous results on albite melt.[22]

The anomalous behavior transport properties could also be explained by a global Arrhenius relation and by empirically expressing the activation volume, $V^*(P,T)$, that varies as a function of pressure and temperature, i.e., $V^*(P, T) = (V_1 + V_2 T) + P\left(V_3 + V_4 T + \frac{V_5}{T}\right)$ such that at high-temperature isotherms, $V^* > 0$ at all pressures, i.e., normal behavior, but at lower-temperature isotherm, the activation volume switches sign, $V^* < 0$ at low pressure to $V^* > 0$ at high pressures (Supporting Text S1, and Table S3).

The anomalous pressure and temperature dependences of the transport properties such as diffusion and viscosity could also be explained using models proposed for super-cooled water, which also exhibits an anomalous transport behavior.[46] Drawing an analogy with the super-cooled water, one could imagine that the albite melt structure is composed of domains of locally favored structure (LFS) that exhibits an anomalous behavior of the transport property. The LFS is hosted within a matrix of normal liquid structure (NLS) that exhibits a normal behavior of the melt transport property. For albite, the LFS is more dominant at low pressures and low temperatures, whereas at high pressures and temperatures, the melt follows a normal behavior, i.e., NLS state. In a melt exhibiting normal behavior, the activation energy required for the diffusion of ions or viscous flow is often associated with the disruption of the local clustering of molecules, and this is associated with an activation energy often associated with an Arrhenian behavior. With the existence of the anomalous domains, i.e., LFS domains, additional activation energy, ΔE_a, is required for molecules participating

Table 3. Coefficients of Transport Properties Including the Pre-Exponential Terms, i.e., D_{x0} and η_0, Activation Energy (E_a), Activation Volume (V_a), and Additional Activation Energy, ΔE_a, As Adopted from the Tanaka Model, i.e., Eqs 11−14 and 16

	diffusivity			η
	D_{Al}	D_{Si}	D_O	η
D_{x0} or η_0 [a]	614 ± 33	497 ± 22	590 ± 7	
E_a (kJ mol^{-1})	126 ± 2	122 ± 2	122 ± 1	90 ± 6
V_a (cm^3 mol^{-1})	1.15 ± 0.06	1.58 ± 0.06	1.22 ± 0.02	3.93 ± 0.18
ΔE_a (kJ mol^{-1})	66 ± 2	75 ± 2	64 ± 1	124 ± 6

[a]Note that the unit for D_{x0} is $\times 10^{-9}$ m^2 s^{-1} and that for η_0 is $\times 10^{-5}$ Pa s.
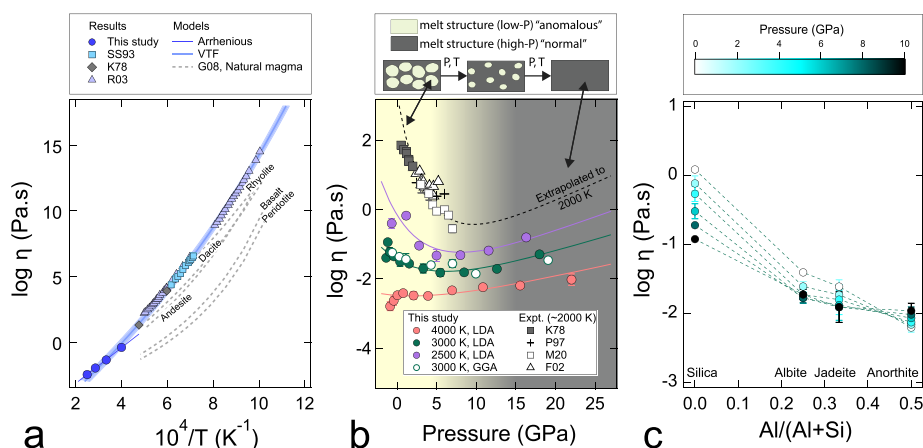

Figure 4. (a) Temperature dependence of viscosity at a constant pressure of ∼0 GPa (blue symbols). Blue thin line represents the Arrhenius relation (Supporting Text S1). Light blue thick line shows the TVF relation describing results from both prior experiments and our FPMD simulations (Supporting Text S1). Also shown are the experimental results at ambient pressure: SS93,[76] and K78.[18] Filled purple triangles represent the viscosity data for albite melt from previous experiments: R03.[54,77−80] Dashed gray lines show the viscosity for naturally occurring magma composition ranging from peridotite to rhyolite. Viscosity of magmatic liquids is calculated using the temperature-dependent TVF model for multicomponent silicate melts.[50] (b) Pressure dependence of viscosity along each isotherm: 4000 K (red symbols), 3000 K (green symbols), and 2500 K (purple symbols). Solid lines represent the fit to the FPMD viscosity data using the Tanaka model (eq 16) (Table 3, Supporting Text S1, and Figure S10). Black dashed line represents the viscosity of albite melt extrapolated to 2000 K using eqs 11−13 and 16. Green open symbols represent the GGA results at 3000 K. Experimental results for albite melt are F02,[19] K78,[18] M02,[17] and P97[20] at 1973, 2000, and 2100 K. The shaded area in panel (b) shows the regions where the pressure-dependent transport properties of albite melt change from anomalous to normal pressure dependence. (c) Viscosity as a function of the Al/(Al + Si) ratio at pressures ranging from 0 to 10 GPa using 2 GPa intervals. Results are for four polymerized melt compositions at a constant temperature of 3000 K.[24,45,47] The symbol color represents the pressure as shown in the color bar. Al/(Al + Si) ratios for silica,[45] albite (this study), jadeite,[24] and anorthite[47] melts are 0, 0.25, 0.33, and 0.5, respectively.

in these structures to flow. Thus, the activation energy of the transport process (diffusion and viscosity) is

$$E_a(T, P) = E_a(P) + \Delta E_a \times S \tag{11}$$

where

$$E_a(P) = E_a + PV_a \tag{12}$$

V_a is the activation volume and "S" refers to the fraction of the anomalous (LFS) domain, which varies as a function of pressure and temperature and is denoted by

$$S = S_0 \exp\left(\frac{\Delta E - P\Delta V}{RT}\right) \tag{13}$$

where S_0 is a prefactor, R is the gas constant, the ΔE and ΔV are likely to be the energy and density differences between the anomalous (LFS) domain and the NLS domains in the albite melt structure, respectively. The negative sign preceding the $P\Delta V$ means that the fraction of the anomalous (LFS) domain reduces at high pressures and temperatures and thus the melt begins to exhibit a normal behavior. The overall pressure- and temperature-dependent self-diffusion behaviors for albite melt could be described as

$$D_x = D_{x0} \exp\left(-\frac{E_a(T, P)}{RT}\right) \tag{14}$$

where D_x is the diffusivity of ionic species, $x = Al, Si, O$; D_{x0} is the pre-exponential factor for the self-diffusion coefficient; R is the gas constant; and $E_a(T, P)$ is the activation energy as defined in eq 12. We note that for Al, Si, and O, $E_a \sim E_O^*(\text{hiP})$ and $\Delta E_a \sim E_O^*(\text{loP}) - E_O^*(\text{hiP})$ (Tables 2 and 3). In this model, to account for the transition from anomalous to normal transport behavior, the fraction of the anomalous (LFS) domain, S, reduces at high pressures and temperatures (Supporting Text S1 and Figure S10).

We find that the self-diffusivities of alkali ions are the fastest, whereas the network-forming ions are the slowest. The self-diffusivity of the ions follows the order $D_{Na} > D_O > D_{Al} > D_{Si}$. At low pressures and 2500 K, Na diffusion is significantly greater than that of other ions, i.e., $D_{Na} \approx 50 \times D_{Si \text{ or } Al}$. However, upon increasing pressure, the self-diffusivity of alkali ions, D_{Na}, reduces more rapidly with increasing pressure, i.e., a positive activation volume, whereas the network-forming ions have a negative activation volume and hence the diffusivity increases with pressure. The large differences in the self-diffusivity of alkali and framework ions change to $D_{Na} \approx 3 \times D_{Si \text{ or } Al}$ at ∼16 GPa and
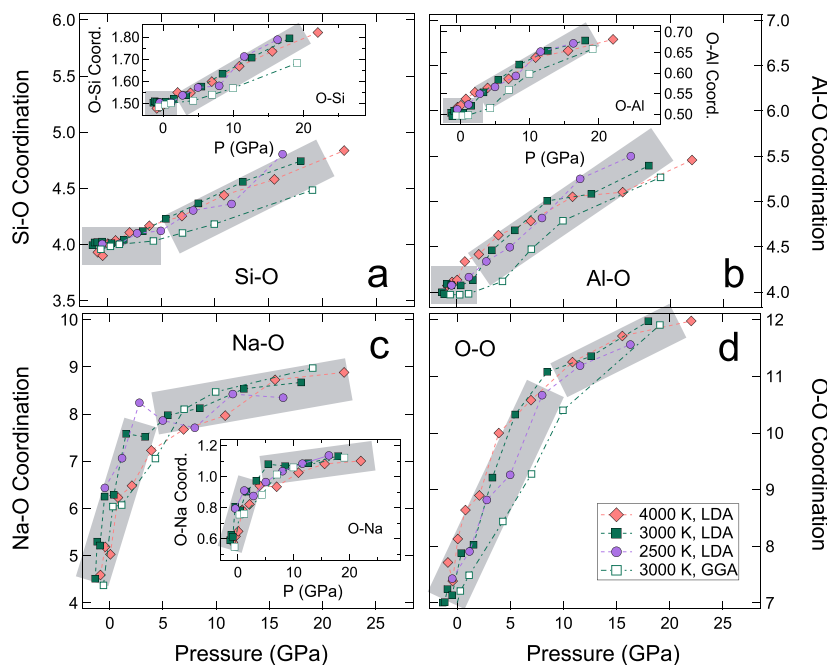
Figure 5. Average cation−oxygen coordination number as a function of pressure for (a) SiO_X, (b) AlO_X, (c) NaO_X, and (d) OO_X at 4000 K (red diamonds with dotted lines), 3000 K (green squares with dotted lines), and 2500 K (purple circles with dotted lines). The inset in panels (a−c) represents the oxygen−cation coordination number for respective ion pairs. Shaded band indicates the discontinuity in the trend of pressure evolution of the coordination environment. And this is likely related to the changes in the internal pressure expressed as interatomic forces (P_{int}^F) (Figure 2). In all figures, the green open squares with dashed and dotted lines represent the average coordination numbers from GGA at 3000 K.

2500 K. Alkali ions are large and often weakly bonded to the oxygen ions. In contrast, the network-forming cations Si or Al are often tightly held by oxygen atoms. A similar pressure dependence of D_{Na} was reported from the previous classical MD simulations.[21,22] We also observe two pressure regimes based on the rate of the decrease of D_{Na}. At the lower-pressure regime (<∼5 GPa), along each isotherm, Na diffusivity decreases by an order of magnitude upon compression from ambient pressure to ∼5 GPa. For example, along the 3000 K isotherm, D_{Na} decreases from 32.3×10^{-9} m^2 s^{-1} at ∼0 GPa to 5.2×10^{-9} m^2 s^{-1} at ∼5 GPa (Figure 3 and Supporting Datasheet). At pressure >∼5 GPa, with increasing pressures, the decrease in Na diffusivity, D_{Na}, is more gradual (Figure 3). In comparison to lower temperatures ∼2500 K, where $\frac{D_{Na}}{D_{Si/Al}} \sim 50$, at 4000 K, $\frac{D_{Na}}{D_{Si/Al}} \sim 6$. Thus, at higher temperatures, the differences between the self-diffusivity of alkali ions and network-forming ion are significantly reduced.[47,48]

Viscosity. We find that the viscosity of albite melt is affected by both temperature and pressures. At ambient pressure, viscosity (η) increases by 2 orders of magnitude when the temperature decreases from 4000 K to 2500 K (Figure 4 and Supporting Datasheet). We have used an Arrhenius relation to describe our melt viscosity data at ambient pressures and find that the extrapolation of the Arrhenius model to lower temperatures deviates significantly from the experimental data for albite melt (Figure 4). Instead, we find that, at zero pressures, the temperature dependence of the viscosity (η) of albite melt is well described by a Tamman−Vogel−Fulcher (TVF) relation

$$\eta = \eta_0 \exp[A(T - T_0)] \tag{15}$$

where η_0, A, and T_0 are constants (Figure 4 and Supporting Text S1). The TVF equation has been successfully used to describe the non-Arrhenian behavior of polymerized melts with diverse compositions including anorthite, jadeite, melts in Na_2O-SiO_2 join, and multicomponent silicate melts.[24,47,49−52]

Similar to diffusivity, we find that the pressure dependence of η is distinct for the low-temperature (2500−3000 K) and high-temperature isotherms (4000 K). At lower isotherms, upon compression to ∼10 GPa, η decreases but upon further compression beyond 10 GPa, the viscosity increases with increasing pressure (Figure 4). Thus, there is a minimum in the pressure dependence of η, which is most pronounced for the low-temperature isotherm 2500 K. The pressure dependence of η exhibit expected trends at 4000 K (Figure 4). The pressure and temperature dependences of η could also be described with the Tanaka model.[46]

$$\eta = \eta_0 \exp\left(\frac{E_a(T, P)}{RT}\right) \tag{16}$$

where η_0 is the pre-exponential viscosity and $E_a(T, P)$ is the activation energy as defined in eq 12. Lower-temperature extrapolation of our simulation result is in excellent agreement with the previous experiments[17−19] (Figure 4).

At a constant temperature of 3000 K, we also explored the effect of composition on η using the viscosity of various polymerized melts from the previous studies.[24,43,52] The degree of polymerization of silicate melt can be defined using the NBO/T ratio. For all of the fully polymerized melt compositions considered here, i.e., silica, albite, jadeite, and anorthite, the NBO/T ratio equals zero. So, we compare the variation in η as a function of the Al/(Al + Si) ratio. For a constant pressure, we find that the η decreases with an increasing Al/(Al + Si) ratio across these melt compositions[24,47,53] (Figure 4). Also, the pressure dependence of viscosity, i.e., $\left(\frac{d\eta}{dP}\right)_T$, increases with an increasing Al/(Al + Si) ratio, which is similar to the previous experimental findings.[54,55]
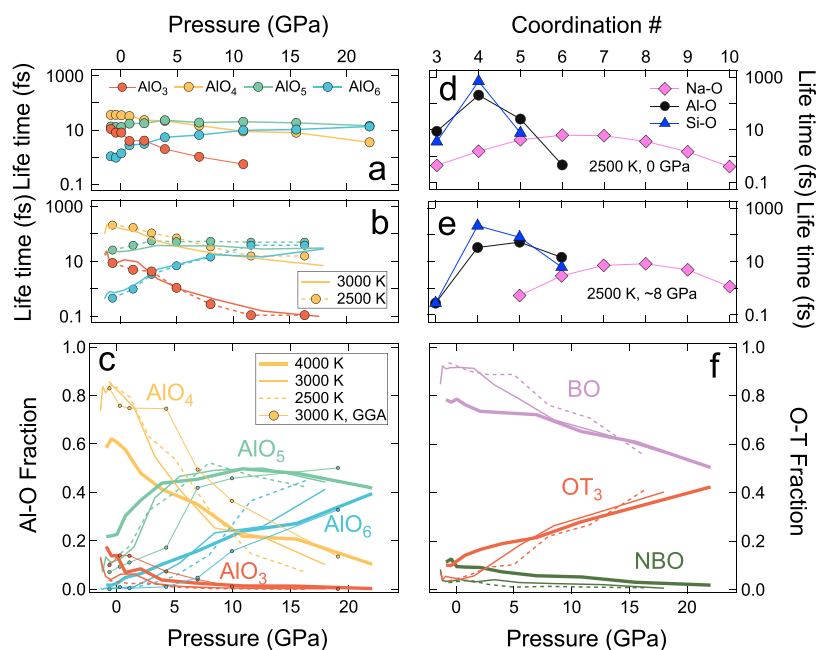
Figure 6. Plots of average lifetime (τ) of the Al−O bonds as a function of pressure at (a) 4000 K and (b) 3000 and 2500 K. (c) Plot of AlO_X species as a function of pressures, at 4000 K (thick lines), 3000 K (thin lines), and 2500 K (dashed lines). In panel (c), the thin line with circles shows the AlO_X species calculated using the GGA method at 3000 K. Average lifetime (τ) for all species: Al−O, Si−O, and Na−O bonds (d) at 2500 K and ∼0 GPa and (e) at 2500 K and ∼8 GPa. The average lifetime (τ) is in femtoseconds (10^{-15} s) and is normalized to 1 ps of simulation time. (f) Plot of the fraction of bridging oxygen ions (BOs), nonbridging oxygen atoms, and oxygen triclusters (OT_3) along each isotherm.

Structure. Upon compression, the melt structure accommodates densification by adjusting bond distances, bond angles, and changes in coordination. For instance, upon compression, the average Na−O coordination (NaO_x) in albite melt increases with a pressure of up to ∼5 GPa; beyond 5 GPa, the NaO_x is rather insensitive to further compression. Upon compression, the coordination environment for O−O also shows a similar trend i.e., there is an initial rapid increase in the coordination followed by a slower rate of increase in the coordination at higher pressure (Figure 5). We find a similar pressure-dependent trend for O−Na coordination (Figure 5). In the lower-pressure regime, the average bond distance for Na−O and O−O also shows a slight increment upon compression (Supporting Figure S11). When the pressure-dependent changes to the coordination environment saturate, the average bond distance decreases with increasing pressure at the high-pressure regime.

Upon compression, the average SiO_X coordination remains constant at up to ∼5 GPa and increases linearly with increasing pressure beyond that (Figure 5). The effect is more pronounced in lower-temperature isotherms compared to that of 4000 K. Within the range of pressures explored in this study, i.e., 0−22 GPa, the average SiO_X does not reach a 6-fold coordinated environment. In contrast to SiO_X, the average AlO_X coordination changes more readily upon compression. At higher temperatures, i.e., 4000 K, the average T−O (T = Si/Al) bond distances increase continuously with increasing pressure to accommodate the continuous changes in the coordination environment. At lower isotherms, i.e., 2500−3000 K, the average T−O bond distance decreases with increasing pressure up to a few gigapascals, and then upon further compression, the average T−O increases to accommodate the changes in the coordination environment (Figures 5 and S11). A similar behavior of the T−O bond length as a function of pressure has been observed in silicate melts with basaltic composition with NBO/T ∼ 0.7.[56]

The effect of pressure on the average coordination number is more pronounced than the effect of temperature (Figure 5). However, the effect of temperature on the relative abundance of individual coordination species is more pronounced (Figure 6). We find that at ambient pressure, the abundance of AlO_4 species are ∼85% at 2500 K, 80% at 3000 K, and only ∼60% at 4000 K. At 4000 K, 3-fold (∼14% AlO_3) and 5-fold (∼22% AlO_5) coordinated aluminum species are much more abundant in comparison to that at the lower isotherms, i.e., <5% AlO_3 and ∼10% AlO_5 (Figure 6). Previous experimental studies using NMR spectroscopy also reported up to ∼30% AlO_5 and ∼8% AlO_6 in albite melt and glasses at high pressures of up to ∼10 GPa and temperature from ∼900 to 1000 K.[13,14] At ambient pressure, the abundance of TO_4 species are ∼95% at 2500 K and ∼90% at 3000 K. At 4000 K, the abundance of TO_4 species are ∼75% and the abundance of TO_3 species are ∼15%. At 0 GPa and lower-temperature isotherms, 3-fold coordinated T is less than ∼5% (Figure 6).

Drawing analogy from crystalline albite, a framework silicate, where all of the oxygen atoms are bridging oxygen atoms (BOs), it is expected that the albite melt should also have mostly BOs at ambient pressures and low temperatures. However, it is likely that as crystalline albite melts, the three-dimensional network of SiO_4 and AlO_4 is partially ruptured producing a fraction of nonbridging oxygen atoms (NBOs), i.e., a small fraction of BOs are converted to NBOs as the crystalline phase melts. NMR spectroscopic studies on aluminosilicate glasses do confirm this and indicate the presence of a small fraction of nonbridging oxygen atoms (NBOs).[13,53] Based on our study, the abundance of different O−T species (e.g., O−T_1 = NBO and O−T_2= BO) also vary widely over the explored range of pressures and temperatures (Figure 6). For instance, at ambient pressures and 4000 K, we find ∼10−12% of NBO atoms. However, at ambient pressures and lower temperatures, the abundance of NBOs are significantly lowered to ∼4% at 3000 K and ∼2% at 2500 K. At

Table 4. Thermodynamic Fit Parameters for the Gibbs Energy Associated with the Speciation Reactions (Eq 17)

equilibrium reaction	ΔS^* (kJ mol^{-1} K^{-1})	ΔV^* (cm^3 mol^{-1})	ΔH^* (kJ mol^{-1})	P_{range} (GPa)	T_{range} (K)
$TO_4 + TO_6 = 2\ TO_5$	9.50×10^{-3}	-0.07	-7.2	$0-24$	$2500-4000$
$AlO_4 + AlO_6 = 2\ AlO_5$	9.62×10^{-3}	0.78	-19.8	$0-24$	$2500-4000$
$OT_1 + OT_3 = 2\ OT_2$	1.27×10^{-2}	1.68	-91.7	$0-24$	$2500-4000$
$NBO + TO_4 = TO_5$	5.58×10^{-3}	-13.00	-11.9	$0-7$	$2500-4000$
$BO + TO_4 = TO_5$	5.70×10^{-4}	-6.75	61.7	$0-24$	$2500-4000$

ambient pressures, the abundance of BOs increase with decreasing temperature, i.e., there are ~80, ~90, and ~93% BOs at 4000, 3000, and 2500 K, respectively. Upon compression, the fraction of NBOs and BOs decrease due to the formation of higher coordinated framework cations via the following reaction mechanisms: $TO_4 + NBO = TO_5$ and $TO_4 + BO = TO_5$.[57] The NBO in the first reaction transforms into a BO attached to TO_5, whereas BO in the second reaction transforms into an oxygen tricluster (OT_3). Thus, as TO_4 attaches to BOs to form OT_3, there is a positive correlation between the abundance of TO_5 and OT_3 (Figure 6).

We evaluate the thermodynamics of the speciation involving BOs, NBOs, TO_4, and TO_5, where the equilibrium constant (K) for a speciation reaction is related to the energetics via the formalism

$$\ln K = -\frac{\Delta G}{RT} = -\frac{\Delta H^* - T\Delta S^* + P\Delta V^*}{RT} \quad (17)$$

The ΔG is the Gibbs free energy associated with the speciation reaction, ΔH^*, ΔS^*, and ΔV^* are the enthalpy, entropy, and volume changes associated with the speciation reaction (Table 4), respectively. We find that the mechanism by which NBOs are often consumed to form TO_5 species is via the speciation reaction $TO_4 + NBO = TO_5$. The energetics, i.e., ΔH^* (-11.9 kJ/mol), ΔV^* (-13 cm^3/mol), and ΔS^* (-5.6 J/(mol K)), of the speciation reactions indicate that this is one of the most favored speciation process that produces TO_5 species at the lower-pressure regime up to ~7 GPa. Beyond 7 GPa, we do not find any NBO species and hence this reaction ceases to operate. Instead, at higher pressures, TO_5 species are produced via the speciation reaction: $TO_4 + TO_6 = 2\ TO_5$, which have a slight negative ΔV^* (-0.1 cm^3/mol) and negative ΔH^* (-7.2 kJ/mol), and this is likely to occur at relatively higher pressures when TO_6 species are available. Similarly, $AlO_4 + AlO_6 = 2\ AlO_5$ have a slight positive ΔV^* (0.8 cm^3/mol) and negative ΔH^* (-19.8 kJ/mol) and is also likely to occur at relatively higher pressures when AlO_6 species are available. The formation of TO_5 and AlO_5 by the combination of tetrahedral and octahedral units is very similar to the perspective of the energetics. The slightly lower ΔV^* for the formation of the TO_5 is offset by the more negative ΔH^* for the formation of AlO_5. It is very likely that this slight variation of ΔV^* and ΔH^* is an artifact and related to the scatter in the speciation data owing to the fact that the species have limited stability over the temperature and pressure ranges. The speciation reaction $TO_4 + BO = TO_5$ has a negative ΔV^* (-6.8 cm^3/mol) and a positive ΔH^* (61.7 kJ/mol); thus, it is likely to only occur when the NBO species are exhausted. The $OT + OT_3 = 2\ OT_2$ has the largest entropy, i.e., ΔS^* (-12.7 J/(mol K)), of all of the reactions considered. This would mean that at high temperatures, the dissociations of triclusters (OT_3) would be favored to form the bridging oxygen atoms, i.e., OT_2 species, and complementary nonbridging oxygen atoms, i.e., OT_1 species (Table 4).

■ DISCUSSION

Upon initial compression, we find that the thermal pressure coefficient $\left(\frac{dP}{dT}\right)_V = \alpha K_T$ and the Grüneisen parameter (γ) of albite melt remain insensitive and then gradually increase linearly (Figure 1). This is related to the structural changes in the polymerized silicate melts. The compression mechanisms involved in melt densification could be a combination of a decrease in the Na–O bond length, an increase in the coordination number, and a decrease in the T–O–T bond angle, i.e., the rearrangement of the network-forming framework with increasing pressure.[12,58] Polymerized melts show a delay in the Al/Si–O coordination increase upon initial compression dictated by tetrahedral packing limit.[59] We find that in albite melts at pressures <5 GPa, the average SiO_X coordination environment remains 4-fold, and the densification is accommodated by the tilting of polyhedral units (Figures 5 and 7). The
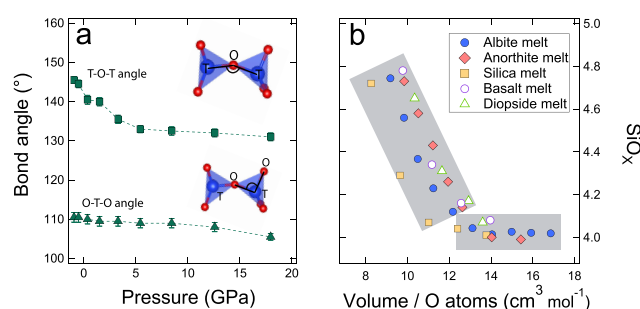

Figure 7. (a) Plot of intertetrahedral T–O–T bond angle and intratetrahedral O–T–O as a function of pressure at 3000 K. (b) Plot of average SiO_X for liquid $NaAlSi_3O_8$ (filled blue circles) at 3000 K as a function of volume normalized to the number of oxygen atoms. The average SiO_X for other silicate melts is also shown for comparison: silica,[45] anorthite,[58] basalt,[67] and diopside.[66] Shaded area is the volume regime where the Si–O coordination remains close to ~4.

structural changes below and above 5 GPa could also be related to the transition in the internal pressure, $P_{int}^F < 0$ to $P_{int}^F > 0$. The changes in the internal pressures are related to the changes in the nature of the interatomic forces from the attractive force regime ($P_{int}^F < 0$) to the repulsive force regime ($P_{int}^F > 0$) (Figure 2) and are also likely to affect the bulk physical properties of dense fluids.[41] The coefficient of thermal expansion (α) and isothermal bulk compressibility (β_T) also show a large reduction at low pressures where the interatomic forces are dominated by attractive forces (Supporting Figure S8). Similarly, at pressures <5 GPa where $P_{int}^F < 0$, the average Na–O and O–O coordinations exhibit a rapid increase, but at pressures >5 GPa, i.e., $P_{int}^F > 0$, the changes in the Na–O and O–O coordinations become more gradual (Figure 5). The average T–O–T bond angle decreases upon compression as observed from the shift of the peak position of the T–O–T bond angle distribution to lower values (Figure 7 and Supporting Figure

S12). We find that at 3000 K and pressures <5 GPa, the T—O—T bond angles decrease rapidly from 146 to 135° at lower pressure, i.e., ~11° (Figure 7). At pressures >5 GPa, the T—O—T bond reduced by ~4° from ~5 to ~18 GPa. Thus, the densification is more effectively achieved by changes in coordination at pressures >5 GPa. The behavior of the albite melt is similar to its crystalline analogue where the alteration of the T—O—T bond angles accommodates the densification of the crystal structure.[60] For pressures <5 GPa, the intratetrahedral bond angle (O—T—O) remains largely unaffected (Figure 7). This near-constant O—T—O angle at a lower pressure is related to the fact that TO_4 behaves as rigid units, i.e., the shapes are largely unaltered. In addition, at low pressures, the predominant species is TO_4, and only when the species evolve to TO_5, the polyhedral units may show a slight variation in the O—T—O angles. Our findings of the pressure evolution of the T—O—T and O—T—O bond angles are similar to the observed behavior in the polymerized aluminosilicate melt of jadeite composition.[59]

Transport properties of albite melt exhibit anomalous pressure and temperature dependences (Figures 3 and 4). Because of the difference in the P/T evolution of self-diffusion coefficient, a distinct diffusion mechanism will operate at different conditions. At high temperatures and ambient condition where all species have similar mobility, the free flow of atoms as a group is the preferable diffusion mechanism. This is sustained by the frequent bond-breaking events and shorter lifetime of those bonds (Figure 6). The average lifetimes for Na—O, Al—O, and Si—O bonds normalized for a 1 picosecond (ps) simulation time are ~18, ~58, and ~135 fs, respectively, at 4000 K. At 2500 K, the lifetime of Na—O is ~24 fs, but the lifetimes of Al—O and Si—O bonds are ~245 and ~714 fs. At low-temperature and/or high-pressure conditions, the network-forming cations, i.e., Si/Al atoms, are bonded to the oxygen atoms and often sluggish in their mobility. In contrast, the Na atoms are relatively weakly bonded to the oxygen atoms and can easily break away and be mobile. Hence, in contrast with Si, Al, and O, which all exhibit anomalous self-diffusivity, i.e., self-diffusivity increases upon compression, the self-diffusivity of the Na atoms exhibits a normal trend, i.e., decreases upon compression (Figure 3). At pressure <5 GPa, D_{Na} reduces more rapidly with increasing pressure. In contrast, at pressure >5 GPa, D_{Na} reduction with pressure is more gradual. This discontinuous behavior in the pressure dependence of the D_{Na} could be explained by the changes in the melt structure. For instance, the pressure evolution of the Na—O coordination also exhibits a discontinuous behavior at ~5 GPa. The O—Na coordination also increases rapidly at lower pressures and remains constant at high pressure (Figure 5). In addition, the Na—Na distances also exhibit discontinuous changes at ~5 GPa (Supporting Figure S13). In contrast, the O—Si/Al coordination exhibits a continuous increase with pressure (Figure 5).

We note that at a high temperature of 4000 K, the viscosity of the albite melt increases sharply up to a few gigapascals and then increases more gradually upon further compression (Figure 4). The sharp increase of viscosity at a lower pressure is similar to the observed behavior of the viscosity of basaltic melt composition.[52] These low-pressure phenomena are very likely caused by the high temperatures where NBOs (~10% at ambient pressure) and TO_3 (~15% at ambient pressure) are relatively more abundant, and thus cause a lower viscosity. Upon compression, once all of the NBOs and TO_3 species are consumed by the formation of TO_4, by combining TO_3 and NBO species, within a few gigapascals, the viscosity increases

more gradually. TO_4 species are dominant at lower pressure and transform into TO_5 by combining with NBOs or BOs, i.e., TO_4 + NBO/BO = TO_5. The transformation of TO_4 to TO_5 involving NBOs is likely to be dominant at low pressures.[57] The lifetimes (τ) of all AlO_X/SiO_X species are short, and all species become less stable at 4000 K compared to that at lower isotherms, i.e., 3000 and 2500 K (Figure 6). The aluminosilicate melts at high temperature thus show a normal pressure dependence, i.e., a decrease in self-diffusion and an increase in viscosity with increasing pressure.

At lower-temperature isotherms (2500 and 3000 K), the η exhibits minima and the diffusivity exhibits maxima (Figures 3 and 4). This anomalous pressure dependence of the transport properties is related to the atomistic scale changes in the melt structure (Figure 6). The abundance of AlO_5 species increase upon compression and exhibit maxima at pressures corresponding to the minima observed in the pressure dependence of the η. Also, the AlO_5 units are less stable compared to the AlO_4 and AlO_6 units. At lower pressures and in low-temperature isotherms, where AlO_4 are the dominant species, we observe $\tau_{AlO_4} > \tau_{AlO_5} > \tau_{AlO_6}$. However, at a mid-pressure range where the abundance of AlO_5 are twice the abundance of AlO_4, $\tau_{AlO_4} \approx \tau_{AlO_5}$ (Figure 6). Previous FPMD studies on the polymerized melt of anorthitic composition suggest that the anomalous transport properties could also be explained by the reduction of the stability of SiO_4 species.[58,61] In our results on albite melts, we find that the lifetime of the Si—O bond for all SiO_X species is typically longer than that of the Al—O bonds for all respective AlO_X species, i.e., $\tau_{SiO_x} > \tau_{AlO_x}$. Although the abundance of SiO_5 species and the corresponding lifetime τ_{SiO_5} increase with increasing pressure, we note that the $\tau_{SiO_4} > \tau_{SiO_5} > \tau_{SiO_6}$ at pressures up to 15 GPa (Supporting Figure S14). Thus, for polymerized melts (albite and anorthite), both the pressure-induced abundance of 5-fold complexes and a large reduction in the lifetime τ_{Si/AlO_4} could account for the decrease in melt viscosity with increasing pressure. The reduction of τ_{Si/AlO_4} would also mean the formation of more 5-fold complexes, which are transient complexes that help the mobility of the oxygen atoms.[20,55,62] Enhanced mobility of oxygen atoms could lead to the reduction of viscosity. We have also explored the relationship between the Si—O bond lifetime for SiO_X species, τ_{SiO_x}, and the relaxation time scale of glasses (τ_∞) by extrapolating the high-temperature FPMD data into lower temperatures relevant for the albite glass transition, i.e., 900—1100 K[63] (Supporting Figure S15). We find that the extrapolated τ_{SiO_x} data to lower temperature qualitatively agrees with the relaxation time scale of glasses, where τ_∞ is estimated with an average viscosity (10^{12} Pa s) and shear moduli at an infinite frequency (~10 GPa) for aluminosilicate glass.[63]

Our result on albite melt is very similar to that of jadeite melt.[24] Transitions to 5-fold and 6-fold coordination polyhedral units are associated with the lengthening of the Al/Si—O bond distances, i.e., weakening of the Al/Si—O bonds (Supporting Figure S11). Structural changes in response to the densification of the melt lead to the weakening of the network structure and an increase in the configurational entropy.[20,62,64,65] This is likely to aid in overcoming the activation barrier, resulting in the enhanced melt mobility upon compression. This is contrary to what would be normally expected upon compression. At pressures beyond the 5-fold coordination changes, the melt is

denser and exhibits a normal behavior of transport properties (Figures 3 and 4).

The upward migration of magma is dependent on the magma mobility $(\Delta\rho/\eta)$,[7,8] where $(\Delta\rho)$ is the contrast in the density of the magma with the surrounding rock and (η) is the viscosity of the magma. The buoyancy $(\Delta\rho)$ of a melt is strongly influenced by the thermodynamic parameters such as K_T, α, and their pressure and temperature dependences. Based on our results on polymerized albitic melt, we find that αK_T exhibits a discontinuous behavior upon compression. A similar behavior of αK_T, i.e., discontinuous pressure dependence, has also been observed in highly polymerized melts including silica and anorthite.[45,58] In contrast, the pressure dependence of αK_T is continuous in depolymerized melts such as diopside and basalt[66,67] (Figure 1). Upon further analysis of the pressure dependence of αK_T, we find that the bulk modulus (K_T) of albite melt increases continuously. The discontinuous pressure dependence of αK_T is due to the behavior of α (Supporting Figure S8). The pressure dependence of α could be best described by an asymptote, i.e., α decreases significantly upon compression at low pressures and then it is insensitive to pressure. This behavior of α is likely to manifest in ascending aluminosilicate magmas, which may have a significant albitic component or polymerized melt fractions. Aluminosilicate magmas may experience extra buoyancy due to a significant change in the α as they upwell toward the surface.

Based on our results on albitic melt, we find that the pressure dependence of viscosity is anomalous, i.e., the viscosity of albitic melt first decreases and then increases upon compression (Figure 4). Aluminosilicate magmas rich in albitic component are likely to be generated in mid- to lower crustal depths of ~15–45 km.[3,68,69] At these mid- to lower crustal depths, the viscosity of the melt with a significant albitic component is likely to be lower than at ambient conditions. In addition, if the melt were to be hydrous, then it is likely to reduce viscosity even further as documented in the recent study on aluminosilicate melt with jadeite composition.[24] The lower viscosity of polymerized silicate melts at mid- to lower crustal depth is likely to enhance mobility. Thus, the time scales of crystal–melt segregation are likely to be reduced. This will further reduce the viscosity of the ascending magma because of an increment in the melt fraction.[69–71] The structural and transport properties discussed for albite melts are relevant for general discussions of the behavior of alkali-bearing magmas with silicic to intermediate composition.

ASSOCIATED CONTENT

Ⓢ Supporting Information

The Supporting Information is available free of charge at https://pubs.acs.org/doi/10.1021/acsearthspace-chem.9b00187.

> Pressure and temperature dependence of the transport properties (Text S1); Differences of the pressure and energy from average values; effect of cell size on the structure of albite melt; log–log plot of mean square displacement; plot of calculated pressures from local density approximation and generalized gradient approximation; isothermal bulk modulus and volume thermal expansion coefficient; Rosenfeld-Tarazona (RT) scaling; the fraction of the locally favored anomalous structure (LFS); intra-tetrahedral (O–T–O) and inter-tetrahedral T–O–T bond angles; plot of average lifetime (τ) of

bonds; average cation–oxygen and Na–Na bond distance (Figures S1–S15). BM3EOS fit parameters; volume-dependent coefficients; and pre-exponential self-diffusion (Tables S1–S4) (PDF)

> Calculated pressures (P), total energies (E), self-diffusion coefficients (D), viscosities (η), and structural properties using LDA/GGA (PDF)

AUTHOR INFORMATION

Corresponding Author
*E-mail: sbajgain@fsu.edu.

ORCID Ⓞ
Suraj K. Bajgain: 0000-0002-8923-8247
Mainak Mookherjee: 0000-0002-0605-5964

Notes
The authors declare no competing financial interest.

ACKNOWLEDGMENTS

REFERENCES

(1) Moyen, J.-F.; Martin, H. Forty years of TTG research. *Lithos* **2012**, *148*, 312–336.

(2) Winther, K. T. An experimentally based model for the origin of tonalitic and trondhjemitic melts. *Chem. Geol.* **1996**, *127*, 43–59.

(3) Huang, W.-L.; Wyllie, P. J. Melting reactions in the system $NaAlSi_3O_8$-$KAlSi_3O_8$-SiO_2 to 35 kilobars, dry and with excess water. *J. Geol.* **1975**, *83*, 737–748.

(4) Boyd, F.; England, J. Effect of pressure on the melting of diopside, $CaMgSi_2O_6$, and albite, $NaAlSi_3O_8$, in the range up to 50 kilobars. *J. Geophys. Res.* **1963**, *68*, 311–323.

(5) Bell, P. M.; Roseboom, E. H., Jr. Melting relationships of jadeite and albite to 45 kilobars with comments on melting diagrams of binary systems at high pressures. *Mineral. Soc. Am., Spec. Pap.* **1969**, *2*, 151–169.

(6) Anovitz, L. M.; Blencoe, J. G. Dry melting of high albite. *Am. Mineral.* **1999**, *84*, 1830–1842.

(7) Stolper, E.; Walker, D.; Hager, B. H.; Hays, J. F. Melt segregation from partially molten source regions: the importance of melt density and source region size. *J. Geophys. Res.: Solid Earth* **1981**, *86*, 6261–6271.

(8) Connolly, J. A.; Schmidt, M. W.; Solferino, G.; Bagdassarov, N. Permeability of asthenospheric mantle and melt extraction rates at mid-ocean ridges. *Nature* **2009**, *462*, 209–212.

(9) Lange, R. A.; Carmichael, I. S. Densities of Na_2O-K_2O-MgO-FeO-Fe_2O_3-Al_2O_3-TiO_2-SiO_2 liquids: New measurements and derived partial molar properties. *Geochim. Cosmochim. Acta* **1987**, *51*, 2931–2946.

(10) Lange, R. A. A revised model for the density and thermal expansivity of K_2O-Na_2O-CaO-MgO-Al_2O_3-SiO_2 liquids from 700 to 1900 K: extension to crustal magmatic temperatures. *Contrib. Mineral. Petrol.* **1997**, *130*, 1–11.

(11) Kress, V. C.; Williams, Q.; Carmichael, I. S. Ultrasonic investigation of melts in the system Na_2O-Al_2O_3-SiO_2. *Geochim. Cosmochim. Acta* **1988**, *52*, 283–293.

(12) Tenner, T. J.; Lange, R. A.; Downs, R. T. The albite fusion curve re-examined: New experiments and the high-pressure density and

compressibility of high albite and NaAlSi3O8 liquid. *Am. Mineral.* **2007**, *92*, 1573−1585.

(13) Allwardt, J. R.; Poe, B. T.; Stebbins, J. F. The effect of fictive temperature on Al coordination in high-pressure (10 GPa) sodium aluminosilicate glasses. *Am. Mineral.* **2005**, *90*, 1453−1457.

(14) Gaudio, S. J.; Lesher, C. E.; Maekawa, H.; Sen, S. Linking high-pressure structure and density of albite liquid near the glass transition. *Geochim. Cosmochim. Acta* **2015**, *157*, 28−38.

(15) Bista, S.; Stebbins, J. F.; Hankins, W. B.; Sisson, T. W. Aluminosilicate melts and glasses at 1 to 3 GPa: Temperature and pressure effects on recovered structural and density changes. *Am. Mineral.* **2015**, *100*, 2298−2307.

(16) McKeown, D.; Galeener, F.; Brown, G., Jr Raman studies of Al coordination in silica-rich sodium aluminosilicate glasses and some related minerals. *J. Non-Cryst. Solids* **1984**, *68*, 361−378.

(17) Mori, S.; Ohtani, E.; Suzuki, A. Viscosity of the albite melt to 7 GPa at 2000 K. *Earth Planet. Sci. Lett.* **2000**, *175*, 87−92.

(18) Kushiro, I. Viscosity and structural changes of albite (NaAlSi3O8) melt at high pressures. *Earth Planet. Sci. Lett.* **1978**, *41*, 87−90.

(19) Funakoshi, K.-i.; Suzuki, A.; Terasaki, H. In situ viscosity measurements of albite melt under high pressure. *J. Phys.: Condens. Matter* **2002**, *14*, 11343.

(20) Poe, B. T.; McMillan, P. F.; Rubie, D. C.; Chakraborty, S.; Yarger, J.; Diefenbacher, J. Silicon and oxygen self-diffusivities in silicate liquids measured to 15 gigapascals and 2800 Kelvin. *Science* **1997**, *276*, 1245−1248.

(21) Bryce, J. G.; Spera, F. J.; Stein, D. J. Pressure dependence of self-diffusion in the NaAlO2-SiO2 system: Compositional effects and mechanisms. *Am. Mineral.* **1999**, *84*, 345−356.

(22) Neilson, R. T.; Spera, F. J.; Ghiorso, M. S. Thermodynamics, self-diffusion, and structure of liquid NaAlSi3O8 to 30 GPa by classical molecular dynamics simulations. *Am. Mineral.* **2016**, *101*, 2029−2040.

(23) Ceperley, D. M.; Alder, B. Ground state of the electron gas by a stochastic method. *Phys. Review Lett.* **1980**, *45*, 566−569.

(24) Bajgain, S.; Peng, Y.; Mookherjee, M.; Jing, Z.; Solomon, M. Properties of hydrous aluminosilicate melt at high pressures. *ACS Earth and Space Chemistry* **2019**, *3*, 390−402.

(25) Liu, M.; Jacob, A.; Schmetterer, C.; Masset, P. J.; Hennet, L.; Fischer, H. E.; Kozaily, J.; Jahn, S.; Gray-Weale, A. From atomic structure to excess entropy: a neutron diffraction and density functional theory study of CaO−Al2O3−SiO2 melts. *J. Phys.: Condens. Matter* **2016**, *28*, No. 135102.

(26) Solomatova, N. V.; Caracas, R.; Manning, C. E. Carbon sequestration during core formation implied by complex carbon polymerization. *Nat. Commun.* **2019**, *10*, No. 789.

(27) Pan, D.; Spanu, L.; Harrison, B.; Sverjensky, D. A.; Galli, G. Dielectric properties of water under extreme conditions and transport of carbonates in the deep Earth. *Proc. Natl. Acad. Sci.* **2013**, *110*, 6646−6650.

(28) Kresse, G.; Hafner, J. Ab initio molecular dynamics for liquid metals. *Phys. Rev. B* **1993**, *47*, 558−561.

(29) Kresse, G.; Furthmüller, J. Efficiency of ab-initio total energy calculations for metals and semiconductors using a plane-wave basis set. *Comput. Mater. Sci.* **1996**, *6*, 15−50.

(30) Kresse, G.; Furthmüller, J. Efficient iterative schemes for ab initio total-energy calculations using a plane-wave basis set. *Phys. Rev. B* **1996**, *54*, 11169.

(31) Nosé, S. A unified formulation of the constant temperature molecular dynamics methods. *J. Chem. Phys.* **1984**, *81*, 511−519.

(32) Kresse, G.; Joubert, D. From ultrasoft pseudopotentials to the projector augmented-wave method. *Phys. Rev. B* **1999**, *59*, 1758.

(33) Allen, M.; Tildesley, D. *Computer Simulation of Liquids*; Clarendon: Oxford, 1987.

(34) Stixrude, L.; Karki, B. Structure and freezing of MgSiO3 liquid in Earth's lower mantle. *Science* **2005**, *310*, 297−299.

(35) Perdew, J. P.; Burke, K.; Ernzerhof, M. Generalized gradient approximation made simple. *Phys. Rev. Lett.* **1996**, *77*, 3865−3868.

(36) Flyvbjerg, H.; Petersen, H. G. Error estimates on averages of correlated data. *J. Chem. Phys.* **1989**, *91*, 461−466.

(37) Daivis, P. J.; Evans, D. J. Comparison of constant pressure and constant volume nonequilibrium simulations of sheared model decane. *J. Chem. Phys.* **1994**, *100*, 541−547.

(38) Nevins, D.; Spera, F. Accurate computation of shear viscosity from equilibrium molecular dynamics simulations. *Mol. Simul.* **2007**, *33*, 1261−1266.

(39) Chen, T.; Smit, B.; Bell, A. T. Are pressure fluctuation-based equilibrium methods really worse than nonequilibrium methods for calculating viscosities? *J. Chem. Phys.* **2009**, *131*, No. 246101.

(40) Oganov, A. R.; Brodholt, J. P.; Price, G. D. Ab initio elasticity and thermal equation of state of MgSiO3 perovskite. *Earth Planet. Sci. Lett.* **2001**, *184*, 555−560.

(41) Kartsev, V.; Shtykov, S.; Pankin, K.; Batov, D. Intermolecular forces and the internal pressure of liquids. *J. Struct. Chem.* **2012**, *53*, 1087−1093.

(42) Rosenfeld, Y.; Tarazona, P. Density functional theory and the asymptotic high density expansion of the free energy of classical solids and fluids. *Mol. Phys.* **1998**, *95*, 141−150.

(43) Ghiorso, M. S.; Nevins, D.; Cutler, I.; Spera, F. J. Molecular dynamics studies of CaAl2Si2O8 liquid. Part II: Equation of state and a thermodynamic model. *Geochim. Cosmochim. Acta* **2009**, *73*, 6937−6951.

(44) Tinker, D.; Lesher, C. E. Self diffusion of Si and O in dacitic liquid at high pressures. *Am. Mineral.* **2001**, *86*, 1−13.

(45) Karki, B. B.; Bhattarai, D.; Stixrude, L. First-principles simulations of liquid silica: structural and dynamical behavior at high pressure. *Phys. Rev. B* **2007**, *76*, No. 104205.

(46) Tanaka, H. A new scenario of the apparent fragile-to-strong transition in tetrahedral liquids: Water as an example. *J. Phys.: Condens. Matter* **2003**, *15*, L703.

(47) Karki, B.; Bohara, B.; Stixrude, L. First-principles study of diffusion and viscosity of anorthite (CaAl2Si2O8) liquid at high pressure. *Am. Mineral.* **2011**, *96*, 744−751.

(48) Fanara, S.; Sengupta, P.; Becker, H.-W.; Rogalla, D.; Chakraborty, S. Diffusion across the glass transition in silicate melts: Systematic correlations, new experimental data for Sr and Ba in calcium-aluminosilicate glasses and general mechanisms of ionic transport. *J. Non-Cryst. Solids* **2017**, *455*, 6−16.

(49) Giordano, D.; Dingwell, D. B. Non-Arrhenian multicomponent melt viscosity: a model. *Earth Planet. Sci. Lett.* **2003**, *208*, 337−349.

(50) Giordano, D.; Russell, J. K.; Dingwell, D. B. Viscosity of magmatic liquids: a model. *Earth Planet. Sci. Lett.* **2008**, *271*, 123−134.

(51) Bauchy, M.; Guillot, B.; Micoulaut, M.; Sator, N. Viscosity and viscosity anomalies of model silicates and magmas: a numerical investigation. *Chem. Geol.* **2013**, *346*, 47−56.

(52) Karki, B. B.; Ghosh, D. B.; Bajgain, S. K. Simulation of Silicate Melts Under Pressure. In *Magmas Under Pressure*; Elsevier, 2018; pp 419−453.

(53) Karki, B. B.; Stixrude, L. First-principles study of enhancement of transport properties of silica melt by water. *Phys. Rev. Lett.* **2010**, *104*, No. 215901.

(54) Scarfe, C. M.; Cronin, D. J. Viscosity-temperature relationships of melts at 1 atm in the system diopside-albite. *Am. Mineral.* **1986**, *71*, 767−771.

(55) Poe, B.; Romano, C.; Zotov, N.; Cibin, G.; Marcelli, A. Compression mechanisms in aluminosilicate melts: Raman and XANES spectroscopy of glasses quenched from pressures up to 10 GPa. *Chem. Geol.* **2001**, *174*, 21−31.

(56) Sakamaki, T.; Suzuki, A.; Ohtani, E.; Terasaki, H.; Urakawa, S.; Katayama, Y.; Funakoshi, K.-i.; Wang, Y.; Hernlund, J. W.; Ballmer, M. D. Ponded melt at the boundary between the lithosphere and asthenosphere. *Nat. Geosci.* **2013**, *6*, 1041−1044.

(57) Morgan, N. A.; Spera, F. J. Glass transition, structural relaxation, and theories of viscosity: A molecular dynamics study of amorphous CaAl2Si2O8. *Geochim. Cosmochim. Acta* **2001**, *65*, 4019−4041.

(58) De Koker, N. Structure, thermodynamics, and diffusion in CaAl2Si2O8 liquid from first-principles molecular dynamics. *Geochim. Cosmochim. Acta* **2010**, *74*, 5657−5671.

(59) Wang, Y.; Sakamaki, T.; Skinner, L. B.; Jing, Z.; Yu, T.; Kono, Y.; Park, C.; Shen, G.; Rivers, M. L.; Sutton, S. R. Atomistic insight into viscosity and density of silicate melts under pressure. *Nat. Commun.* **2014**, *5*, No. 3241.

(60) Mookherjee, M.; Mainprice, D.; Maheshwari, K.; Heinonen, O.; Patel, D.; Hariharan, A. Pressure induced elastic softening in framework aluminosilicate-albite ($NaAlSi_3O_8$). *Sci. Rep.* **2016**, *6*, No. 34815.

(61) Ni, H.; Hui, H.; Steinle-Neumann, G. Transport properties of silicate melts. *Reviews of Geophysics* **2015**, *53*, 715−744.

(62) Yarger, J.; Smith, K.; Nieman, R.; Diefenbacher, J.; Wolf, G.; Poe, B.; McMillan, P. Al coordination changes in high-pressure aluminosilicate liquids. *Science* **1995**, *270*, 1964−1967.

(63) Liu, S.; Pines, A.; Brandriss, M.; Stebbins, J. Relaxation mechanisms and effects of motion in albite ($NaAlSi_3O_8$) liquid and glass: a high temperature NMR study. *Physics and Chemistry of Minerals* **1987**, *15*, 155−162.

(64) Whittington, A. G.; Bouhifd, M. A.; Richet, P. Amorphous Materials: Properties, Structure, and Durability: The viscosity of hydrous $NaAlSi_3O_8$ and granitic melts: Configurational entropy models. *Am. Mineral.* **2009**, *94*, 1−16.

(65) Scamehorn, C.; Angell, C. Viscosity-temperature relations and structure in fully polymerized aluminosilicate melts from ion dynamics simulations. *Geochim. Cosmochim. Acta* **1991**, *55*, 721−730.

(66) Sun, N.; Stixrude, L.; Koker, N. D.; Karki, B. B. First principles molecular dynamics simulations of diopside ($CaMgSi_2O_6$) liquid to high pressure. *Geochim. Cosmochim. Acta* **2011**, *75*, 3792−3802.

(67) Bajgain, S.; Ghosh, D. B.; Karki, B. B. Structure and density of basaltic melts at mantle conditions from first-principles simulations. *Nat. Commun.* **2015**, *6*, No. 8578.

(68) Skjerlie, K. P.; Johnston, A. D. Fluid-absent melting behavior of an F-rich tonalitic gneiss at mid-crustal pressures: implications for the generation of anorogenic granites. *J. Petrol.* **1993**, *34*, 785−815.

(69) Petford, N.; Cruden, A.; McCaffrey, K.; Vigneresse, J.-L. Granite magma formation, transport and emplacement in the Earth's crust. *Nature* **2000**, *408*, 669−673.

(70) Dingwell, D. B.; Mysen, B. O. Effects of water and fluorine on the viscosity of albite melt at high pressure: a preliminary investigation. *Earth Planet. Sci. Lett.* **1985**, *74*, 266−274.

(71) Schmidt, M. W. Melting of pelitic sediments at subarc depths: 2. Melt chemistry, viscosities and a parameterization of melt composition. *Chem. Geol.* **2015**, *404*, 168−182.

(72) Lange, R. A. Temperature independent thermal expansivities of sodium aluminosilicate melts between 713 and 1835 K. *Geochim. Cosmochim. Acta* **1996**, *60*, 4989−4996.

(73) Angel, R. J. Equations of state of plagioclase feldspars. *Contrib. Mineral. Petrol.* **2004**, *146*, 506−512.

(74) Fei, Y. Thermal expansion. *Mineral Physics and Crystallography: a Handbook of Physical Constants* **1995**, *2*, 29−44.

(75) Benusa, M. D.; Angel, R. J.; Ross, N. L. Compression of albite, $NaAlSi_3O_8$. *Am. Mineral.* **2005**, *90*, 1115−1120.

(76) Stein, D. J.; Spera, F. J. Experimental rheometry of melts and supercooled liquids in the system $NaAlSiO_4$-SiO_2: Implications for structure and dynamics. *Am. Mineral.* **1993**, *78*, 710−723.

(77) Russell, J.; Giordano, D.; Dingwell, D. High-temperature limits on viscosity of non-Arrhenian silicate melts. *Am. Mineral.* **2004**, *88*, 1390−1394.

(78) Sipp, A.; Bottinga, Y.; Richet, P. New high viscosity data for 3D network liquids and new correlations between old parameters. *J. Non-Cryst. Solids* **2001**, *288*, 166−174.

(79) Hummel, W.; Arndt, J. Variation of viscosity with temperature and composition in the plagioclase system. *Contrib. Mineral. Petrol.* **1985**, *90*, 83−92.

(80) Urbain, G.; Bottinga, Y.; Richet, P. Viscosity of liquid silica, silicates and alumino-silicates. *Geochim. Cosmochim. Acta* **1982**, *46*, 1061−1072.